

## CHARACTERIZATION OF MICROBIALLY Fe(III)-REDUCED NONTRONITE: ENVIRONMENTAL CELL-TRANSMISSION ELECTRON MICROSCOPY STUDY

JIN-WOOK KIM<sup>1,\*</sup>, YOKO FURUKAWA<sup>1</sup>, TYRONE L. DAULTON<sup>1</sup>, DAWN LAVOIE<sup>2</sup> AND STEVEN W. NEWELL<sup>1</sup>

<sup>1</sup> Marine Geosciences Division, Naval Research Laboratory, Stennis Space Center, MS 39529, USA

<sup>2</sup> US Geological Survey, Reston, VA 20192, USA

**Abstract**—Microstructural changes induced by the microbial reduction of Fe(III) in nontronite by *Shewanella oneidensis* were studied using environmental cell (EC)-transmission electron microscopy (TEM), conventional TEM, and X-ray powder diffraction (XRD). Direct observations of clays by EC-TEM in their hydrated state allowed for the first time an accurate and unambiguous TEM measurement of basal layer spacings and the contraction of layer spacing caused by microbial effects, most likely those of Fe(III) reduction. Non-reduced and Fe(III)-reduced nontronite, observed by EC-TEM, exhibited fringes with mean  $d_{001}$  spacings of 1.50 nm (standard deviation,  $\sigma = 0.08$  nm) and 1.26 nm ( $\sigma = 0.10$  nm), respectively. In comparison, the same samples embedded with Nanoplast resin, sectioned by microtome, and observed using conventional TEM, displayed layer spacings of 1.0–1.1 nm (non-reduced) and 1.0 nm (reduced). The results from Nanoplast-embedded samples are typical of conventional TEM studies, which have measured nearly identical layer spacings regardless of Fe oxidation state. Following Fe(III) reduction, both EC- and conventional TEM showed an increase in the order of nontronite selected area electron diffraction patterns while the images exhibited fewer wavy fringes and fewer layer terminations. An increase in stacking order in reduced nontronite was also suggested by XRD measurements. In particular, the ratio of the valley to peak intensity ( $v/p$ ) of the 1.7 nm basal 001 peak of ethylene glycolated nontronite was measured at 0.65 (non-reduced) and 0.85 (microbially reduced).

**Key Words**—EC-TEM, Layer Contraction, Microbial Fe(III) Reduction, Nontronite, *Shewanella oneidensis*, XRD.

### INTRODUCTION

It has been proposed that oxidation-reduction reactions of layer silicates play an important role in environmental processes including microbial activity, nutrient cycling, plant growth, contaminant migration and diagenetic transformations (*e.g.* Egashira and Ohtsubo, 1983). The first observation that reduced clays swelled less than oxidized forms was in the study of Wyoming bentonite by Foster (1953). Other early studies observed that swelling pressures of ferruginous clays are related to the *b* dimension of the unit-cell (Ravina and Low, 1972, 1977) which was dependent on the oxidation state of octahedral Fe (Kohyama *et al.*, 1973). Subsequent work reported that reduction of Fe(III) in ferruginous clays, amongst other effects, decreased swelling pressures (Egashira and Ohtsubo, 1983; Stucki *et al.*, 1984; Gates *et al.*, 1993), increased cation fixation (Chen *et al.*, 1987; Khaled and Stucki, 1991), smaller specific surface areas (Lear and Stucki, 1989; Shen *et al.*, 1992), and a decrease in mean layer spacing (Wu *et al.*, 1988, 1989). All of these point towards an increase in the interlayer force which is produced by the mutual attraction of net-negatively charged clay interlayer surfaces to the interlayer cations. Increase in interlayer force can be driven by reduction-

induced changes in total clay charge which affects the net negative charge present on layer surfaces. However, this theory has not been fully evaluated because the few direct measurements of clay layer spacings at different redox states that have been performed are inconclusive.

Stucki and Tessier (1991) examined chemically reduced Fe-rich smectite by high resolution (HR)-TEM. Specimens were prepared by thin sectioning after water exchange and resin infiltration following the method of Tessier (1984). Using selected area electron diffraction (SAED), they showed that the crystal stacking changed from turbostratic to a more ordered structure in the reduced state, indicating an increase of interlayer attraction due to the reduction of Fe(III) to Fe(II). However, the expected contraction in layer spacing was not found; rather a constant layer spacing of 1.26 nm was observed in both the oxidized and reduced smectite. This is in conflict with the earlier *in situ* pressure-cell XRD work of Wu *et al.* (1989) which observed a significant decrease in mean interlayer spacing upon Fe(III) reduction in Na-nontronite bulk samples. The effects of resin infiltration on the interlayer spacing are uncertain and the homogeneous layer spacing observed by Stucki and Tessier (1991) were thought to have been artifacts induced by resin infiltration. Furthermore, previous studies focused on chemically reduced smectite using inorganic reductants, such as dithionite (*e.g.* Foster, 1953; Lear and Stucki, 1989; Shen *et al.*, 1992; Drits and Manceau, 2000) which are not likely to occur in abundance or to play a significant

\* E-mail address of corresponding author:

jkim@nrlssc.navy.mil

DOI: 10.1346/CCMN.2003.0510403

role in iron reduction in natural soil environments (Stucki *et al.*, 1987; Gates *et al.*, 1993; Kostka *et al.*, 1996). On the other hand, bacteria have been shown to reduce octahedral Fe(III) effectively in clays (Wu *et al.*, 1988; Gates *et al.*, 1993; Kostka *et al.*, 1999) and are ubiquitous in soil and sediments. In order to understand diagenetic changes of clays in anoxic soil and sediments, it is necessary to study microbe/clay interactions on a nm scale.

The purpose of this study is to demonstrate, using advanced techniques, the changes in the microstructure of ferruginous clays that are induced by metal-reducing bacteria. Structural Fe(III) in nontronite was microbially reduced under anaerobic conditions by *Shewanella oneidensis*, a dissimilatory metal-reducing bacterium. The resulting changes in clay microstructure were determined by comparison with a non-reduced control. In particular, basal layer spacings of non-reduced and reduced nontronite were measured directly using EC-TEM and the results were compared to those of conventionally prepared specimens. The EC-TEM allowed observation of the clays in their hydrated 'native' state, avoiding uncertainties in structural modifications produced by specimen preparation. In addition, changes in nontronite stacking order after microbial Fe(III) reduction were characterized using XRD.

## MATERIALS AND METHODS

### *Clay mineral preparation*

Nontronite from Uley graphite mine, South Australia (The Clay Minerals Society standard, N<sub>Au</sub>-1) (Keeling *et al.*, 2000), was used in this study. Powdered specimens (grain-size <2.0 µm) were sterilized by a 5 min exposure to microwave radiation (Keller *et al.*, 1988), and sterility was confirmed from lack of bacterial growth on Luria-Bertani (LB) agar (Difco, Becton Dickinson Microbiology Systems, Sparks, MD) following a 48 h incubation at 22°C in the dark under aerobic conditions. Note that no chemical treatment was carried out during grain-size fractionation or following that procedure (*e.g.* as in cation exchange). Thus, the clay can be regarded as being minimally processed, and as such, largely in its natural state.

### *Bacterial cultures*

*Shewanella oneidensis* previously isolated from anoxic sediment (Myers and Nealson, 1988) was maintained aerobically on LB agar at 22°C in the dark. The conditions for clay reduction experiments were modified from Kostka *et al.* (1996) and are as follows: a single, well-isolated colony was grown aerobically overnight at 22°C in liquid LB medium and harvested by centrifugation. The culture was introduced to anaerobic conditions incrementally by re-suspension in sterile minimal (M1) medium (pH 7.4) prepared accord-

ing to Myers and Nealson (1988), supplemented with 20 mM formate as the electron donor and 80 mM Fe(III) citrate as the terminal electron acceptor (TEA). The culture was then incubated for 72 h at 22°C under anaerobic conditions. Bacteria were pelleted by centrifugation, washed twice with M1 media, and transferred into 15 mL of fresh M1 media containing 20 mM formate to a density of a 0.5 MacFarland Standard ( $1.5 \times 10^8$  cells mL<sup>-1</sup>). Six milligrams of sterilized nontronite (0.4 mg mL<sup>-1</sup>) were added as the sole TEA and a 5 mL aliquot was placed into a sterile 50 mL centrifuge tube. Controls containing heat-killed bacterial cells and M1 media plus formate were prepared from the same nontronite sample. The tubes were loosely capped and incubated anaerobically in an anaerobic chamber for 4 days at 22°C.

### *Environmental cell transmission electron microscopy*

A JEOL JEM-3010 transmission electron microscope operating at 300 keV with a LaB<sub>6</sub> filament was used in this study. This instrument was equipped with a JEOL area scanning imaging device (ASID), Noran energy dispersive X-ray spectroscopy (EDXS) system, Gatan 764 multi-scan camera (MSC), and Gatan imaging filter (GIF200) capable of electron energy loss spectroscopy (EELS). The microscope was also equipped with conventional single- and double-tilt specimen holders for conventional TEM as well as a state-of-the-art JEOL EC-TEM system. All lattice images were obtained at 250 k magnification with a 20 µm objective aperture.

The EC-TEM system used in this study was described in Daulton *et al.* (2001) and is of the closed-cell design (Fukami *et al.*, 1991). The system is equipped with two interchangeable JEOL EC specimen holders (a two-line gas EC and a four-line gas/liquid EC) that are connected to the EC-TEM system by flexible, stainless steel lines. Both *in situ* EC-TEM specimen holders are capable of circulating gas through the specimen chamber using two lines. The gas can be saturated with water vapor enabling hydrated specimens to be examined in their 'natural' wet state. The four-line holder has two additional service lines that can be used to inject several µL of liquids independently from different reservoirs (these were not used in this study). Each EC holder consists of a small cylindrical cell sealed by two electron transparent windows on the top and bottom. Each window is a 15–20 nm thick amorphous carbon (a-C) film covering seven hexagonally arrayed 0.15 mm apertures on a 3.5 mm diameter Cu disk. Prior to use, the windowed grids were tested to withstand a pressure differential of 250 Torr for 60 s. The EC-TEM system is fully computer controlled facilitating the insertion and retraction of EC holders from the microscope column without breaching the delicate windows.

For EC-TEM studies, the culture was centrifuged, supernatant liquid removed, the pellet rinsed with H<sub>2</sub>O, then re-suspended, and an aliquot (<15 µL) was loaded

on the lower EC window (the rinse procedure prevents salt precipitation on the EC window as the aliquot evaporates). The EC holder was then sealed and inserted into the TEM column. A flow of N<sub>2</sub> gas (2 Torr-L-min<sup>-1</sup>) saturated with water vapor was maintained in the EC during operation at pressures between 10 and 100 Torr. For conventional TEM, specimens were embedded in Nanoplast, which is a hydrophilic resin that can be used with aqueous samples without solvent exchange procedures (Leppard *et al.*, 1996). Embedded specimens were sectioned to 70 nm thickness using a Leica Ultracut UCT microtome.

#### X-ray diffraction

X-ray diffraction analyses were performed on ethylene glycolated (non-reduced and microbially reduced) nontronite (grain-size <2 μm) with a Philips automated diffractometer utilizing CuKα radiation at the University of New Orleans. To minimize re-oxidation of reduced nontronite during XRD measurements, X-ray scans were restricted to a small range of 2θ angles (3–8°) at a scan speed of 1°/min.

## RESULTS

#### Direct measurement of lattice fringes

Following 72 h of incubation of *S. oneidensis* with nontronite, a substantial color change of the clay occurs (tube c) in comparison to the controls of pure nontronite (tube a) and nontronite with cell-free media (tube b) as shown in Figure 1. This color change suggests reduction of the clay in the samples containing viable microbes

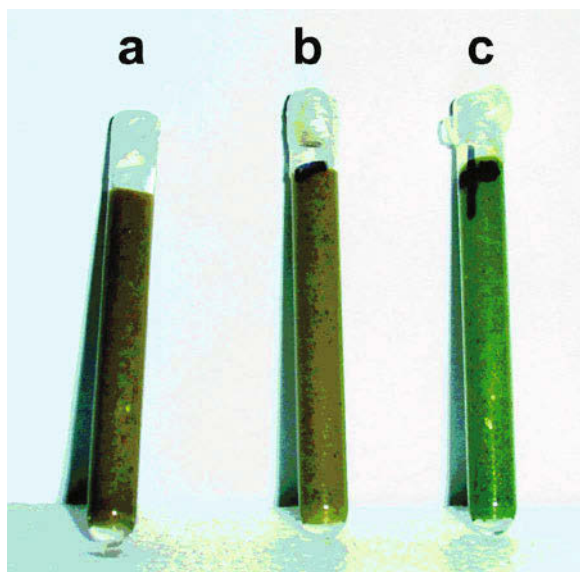


Figure 1. Color changes (tan to green) of nontronite samples after 72 h of incubation with *S. oneidensis* (tube c) in comparison with pure nontronite (tube a) and nontronite with cell-free media (tube b).

when the following two points are considered. The only significant terminal electron acceptor (TEA) present in the cultures was the Fe(III) in the nontronite, and the reduced clay reverted to its original color after several weeks of exposure to ambient conditions (not illustrated here).

Figure 2 shows EC-TEM images for the *S. oneidensis* (S) and nontronite (Nont) culture. Figure 2a is an intermediate-magnification whereas Figure 2b is an enlarged image of the outlined portion of Figure 2a. Examination by EC-TEM shows the typical rod-shaped morphology of *S. oneidensis*. In particular, the bacterial membranes are intact and show no evidence of rupture by partial decompression in the TEM column. The *S. oneidensis*, ranging in length from 2 to 5 μm, were locally distributed in clay aggregates.

Representative, high-resolution lattice fringe images of hydrated clays taken by EC-TEM are shown in Figures 3a (non-reduced nontronite) and 3b (microbially Fe(III)-reduced nontronite). In Figure 3a the non-reduced nontronite shows hydrated layers with spacings varying from 1.5 to 1.6 nm, clearly distinct from 1.0–1.1 nm previously reported for dehydrated layers (*e.g.* Ahn and Peacor, 1986; Lee and Peacor, 1986). Furthermore, 1.5 nm lattice fringes are dominant in most areas of that image while 1.6 nm spacings were observed as one- or two-layer units. The wavy structure and layer termination are abundant, resulting in interfingered layers and non-parallelism in anastomosing layers, and varied spacings along layers. The inset SAED pattern corresponding to the lattice image of Figure 3a shows diffuse basal reflections forming ring patterns. The presence of variable layer spacings and layer non-parallelism results in the diffuseness parallel to *c*\* and normal to *c*\*, respectively. In the example of Figure 3b, the microbially reduced nontronite exhibits fringes that consistently have layer spacings of 1.2–1.3 nm and are readily differentiated from those of the non-reduced nontronite. As shown in Figure 3, fewer wavy fringes and fewer layer terminations were observed in reduced nontronite in comparison with non-reduced nontronite. Unlike the SAED pattern of the non-reduced nontronite, the SAED pattern of the reduced nontronite is not continuous (Figure 3b), although both show diffuse intensity. In comparison, representative lattice fringe images taken by conventional TEM of Nanoplast-embedded nontronite are shown in Figure 4. Importantly, contrary to observations by EC-TEM of hydrated specimens, both the embedded non-reduced (Figure 4a) and reduced (Figure 4b) nontronite show very similar layer spacings (1.0–1.1 nm). In the example of Figure 4a, non-reduced layer spacings of 1.1 nm are dominant with a similar structure previously described above, and the inset SAED pattern displays diffuse basal reflections with *d*<sub>001</sub> values of 1.1 nm. A few nontronite units with 1.0 nm spacings are also observed in Figure 4a. In the example of Figure 4b,

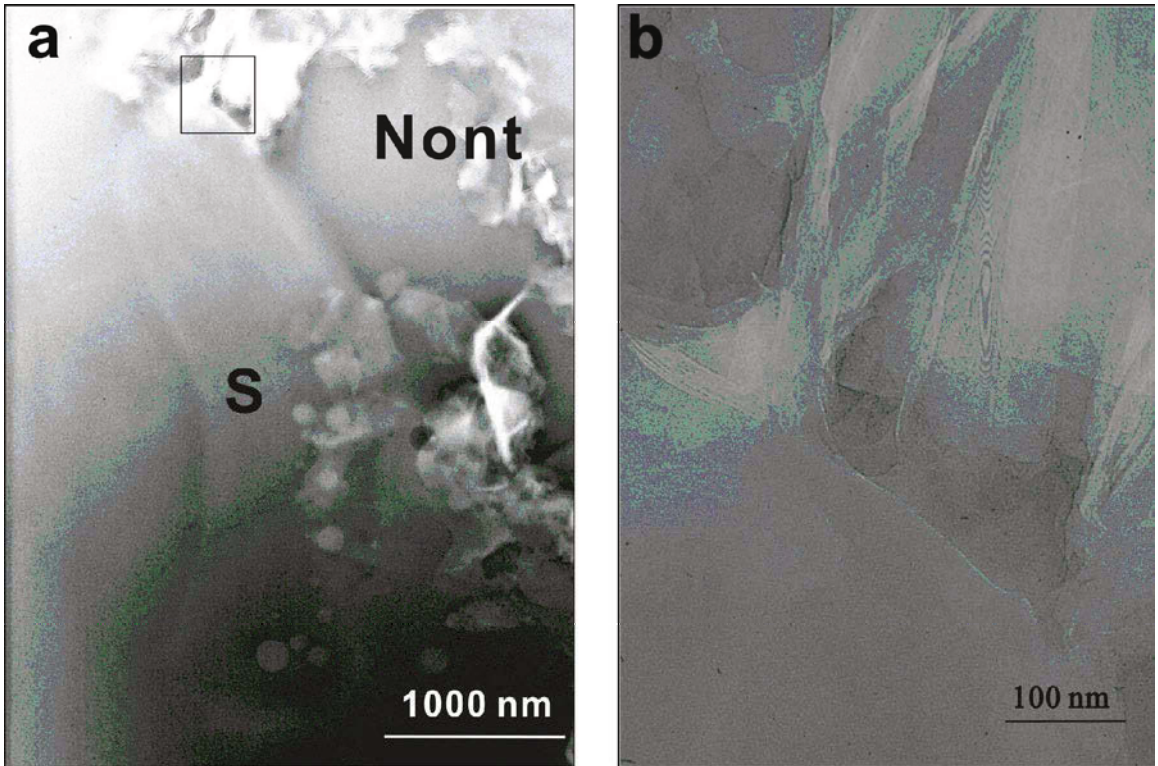


Figure 2. EC-TEM images of *S. oneidensis* (S) with nontronite (Nont) particles, (a) intermediate-magnification image and (b) enlarged image of the outlined portion of (a).

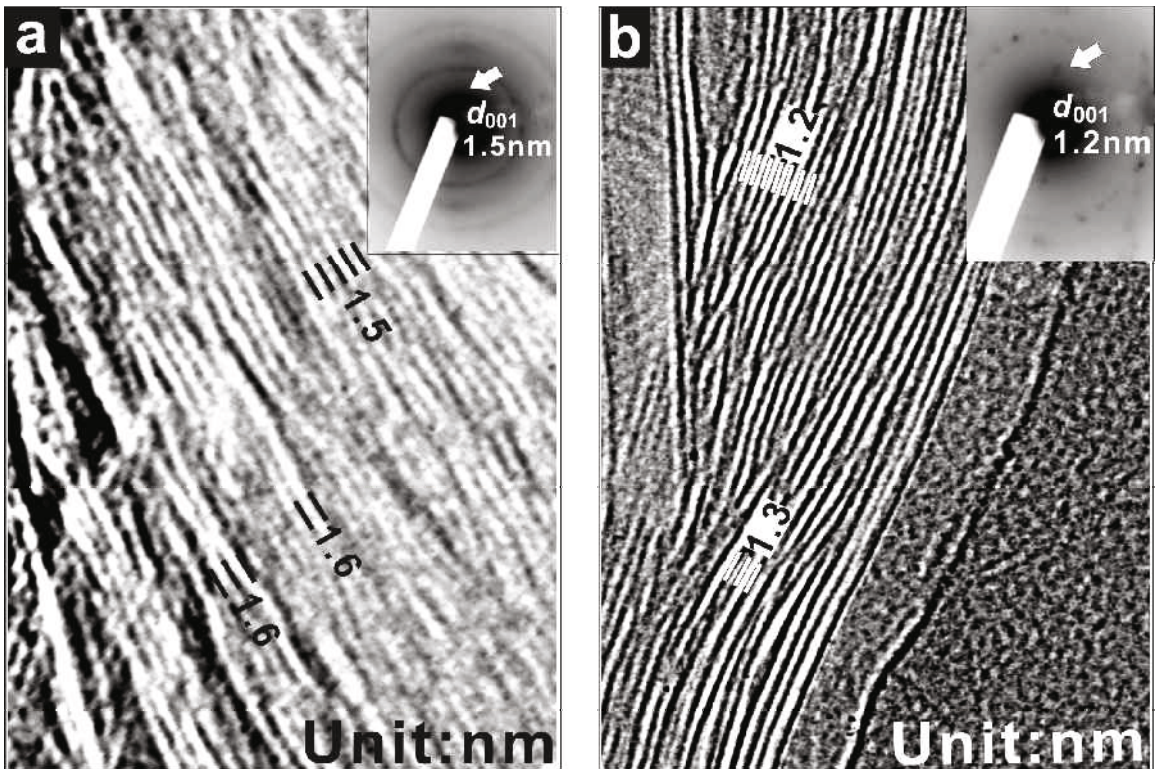


Figure 3. EC-TEM lattice fringe images of (a) non-reduced and (b) microbially Fe(III)-reduced nontronite. SAED patterns of nontronite are shown inset.

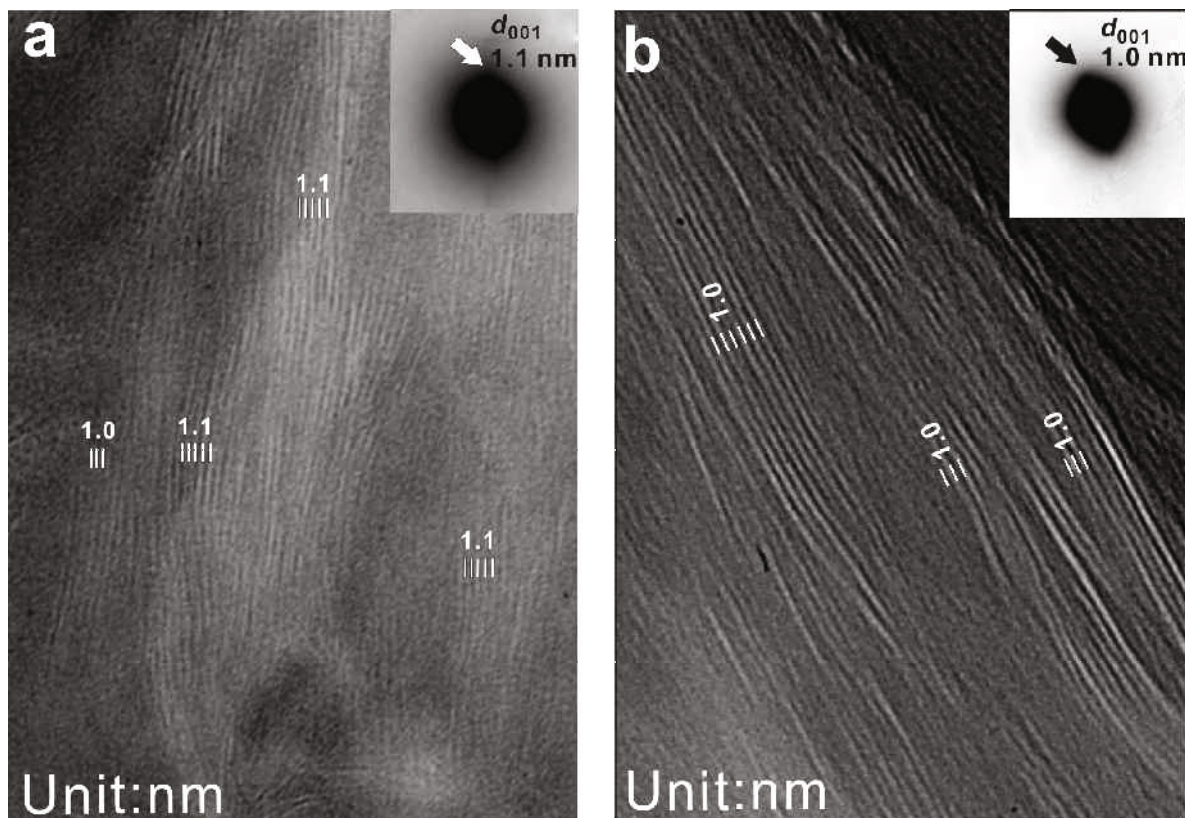


Figure 4. Conventional TEM lattice fringe images of Nanoplast-embedded (a) non-reduced and (b) microbially Fe(III)-reduced nontronite. SAED patterns of nontronite are shown inset.

reduced nontronite exhibits rather continuous lattice fringes with 1.0 nm spacings and corresponding SAED patterns with  $d_{001}$  values of 1.0 nm.

#### Distribution of $d_{001}$ spacing

The distribution of  $d_{001}$  spacings of non-reduced and reduced nontronite imaged by EC-TEM was measured from lattice fringes of 120 and 138 packets of nontronite grains, respectively. The distributions are displayed as accumulate percentages in Figure 5. Each data point represents the average layer spacing of a single packet of a nontronite grain (*i.e.* thickness of nontronite packet divided by number of layers in the packet). The two distributions differ substantially. The population of clay packets in the non-reduced nontronite with layer spacings  $\geq 1.54$  nm ( $\sim 40\%$  of population) are completely absent in the reduced nontronite. Furthermore,  $\sim 58\%$  of clay packets in the reduced nontronite have spacings below the smallest spacing observed in the non-reduced nontronite distribution (1.30 nm). The non-reduced nontronite has a mean layer spacing of 1.50 nm with a standard deviation ( $\sigma$ ) of 0.08 nm, while the reduced nontronite has a mean layer spacing of 1.26 nm with a  $\sigma = 0.10$  nm.

The means of layer spacings for non-reduced and reduced nontronite (Figure 5) differ from one another by  $>2\sigma$ . Therefore, a contraction of 0.24 nm in mean 001 layer spacing of nontronite was observed following Fe(III) reduction. Our measurement is in close agreement with previous *in situ* XRD studies which observed an interlayer contraction of  $0.28 \pm 0.04$  nm,  $d_{100}$  1.95 nm  $\rightarrow$  1.67 nm (for all pressures between 1 and 10 atm), in Na-nontronite (from Garfield, Washington) after  $\sim 85\%$  of the Fe(III) was reduced (based on Figure 8 of Wu *et al.*, 1989).

#### XRD measurement

The XRD data for ethylene glycolated nontronite, non-reduced and microbially Fe(III)-reduced, are displayed in Figures 6a and 6b, respectively. As a measure of crystal order, the ratio of the valley to peak intensity ( $v/p$ ) was measured for the basal layer 001 peak of ethylene glycolated (1.7 nm) nontronite (following the technique of Biscaye, 1965). In that technique,  $p$  (peak) is the peak intensity minus background;  $v$  (valley) is the depression prior to the peak (*i.e.* intensity difference between peak apex and valley preceding the peak). The  $v/p$  ratio of reduced nontronite (0.85) is greater than that of non-reduced nontronite (0.65), indicating higher order in stacking sequence.

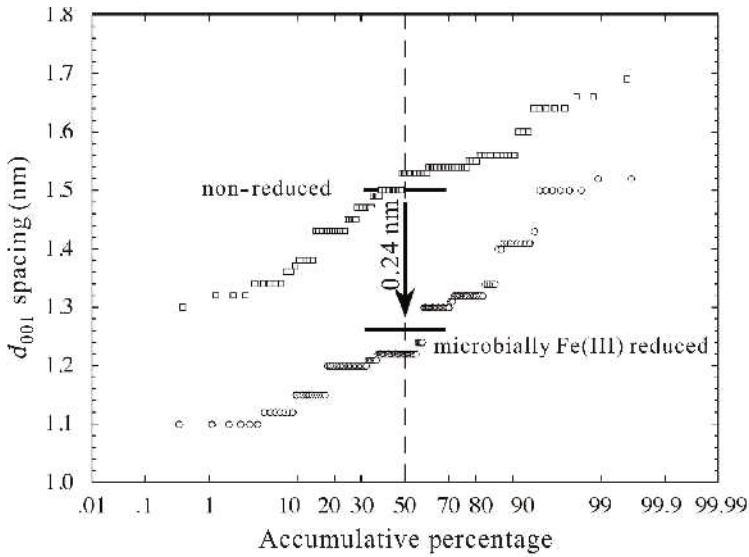


Figure 5. Distribution of 001 layer spacings in non-reduced and microbially Fe(III)-reduced nontronite as measured by EC-TEM. The horizontal axis is scaled to the normal probability distribution (*i.e.* Gaussian distributions plot as straight lines) and represents the value of the integral (normalized to 100%) of the distribution from 0 to  $y$ .

DISCUSSION

We have demonstrated, for the first time by direct TEM measurement, the microbially induced contraction of nontronite basal layers, most likely driven by Fe(III) reduction. This is possible because the clays were examined in their ‘natural’ hydrated state in an environ-

mental cell circumventing dehydration and resin artifact effects of conventional TEM specimen preparation. In previous studies, water exchange with methanol and infiltration with L.R. White resin were used to prevent clay layers from collapsing due to dehydration during TEM examination (Stucki and Tessier, 1991). This

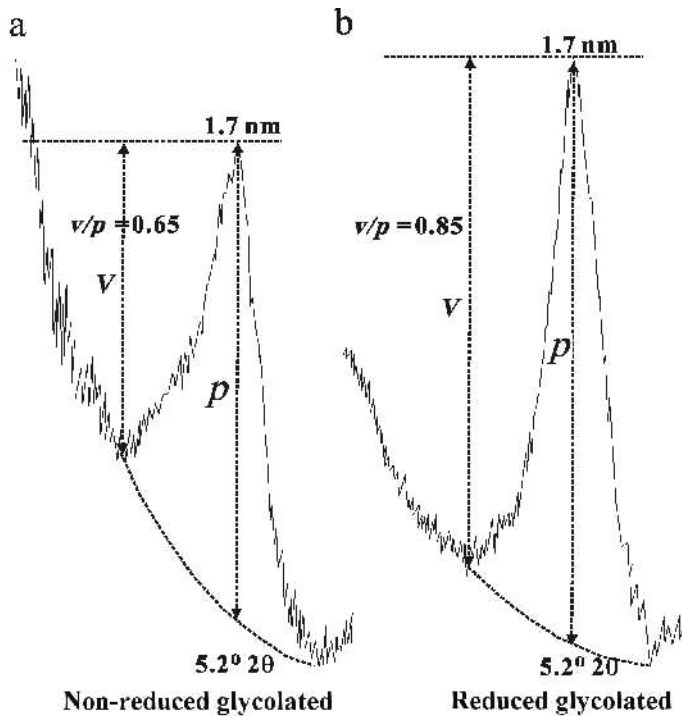


Figure 6. XRD patterns for ethylene glycolated (a) non-reduced control and (b) microbially Fe(III)-reduced nontronite. The heights of the  $v$  (valley) and  $p$  (peak) of the 1.7 nm reflection are shown by arrows.

technique was also adapted to differentiate smectite layers from illite and smectite mixed layers using TEM (Kim *et al.*, 1995). However, the homogeneous layer spacing observed by Stucki and Tessier (1991) in both reduced and non-reduced smectite illustrates the limitations of conventional TEM and infiltration techniques. Their observation is representative of a clay-methanol/resin system which is largely unaffected by the Fe oxidation state, rather than a natural clay-water system.

In Nanoplast-embedded samples, water was directly replaced by resin without the intermediate steps of solvent replacement. However, the difference in layer spacings between Nanoplast-embedded reduced and non-reduced nontronite is too small to provide meaningful information on the contraction of layers induced by microbial effects (most likely those of Fe(III) reduction). Either dehydration in the TEM column or the presence of resin in the interlayers induced contraction of the clay layers precluding accurate measurement of microbially induced layer contraction. In any event, embedding altered the clay interlayer structure thereby precluding measurement of the effects of Fe(III) reduction on layer spacing.

The range of measured basal layer spacings in nontronite (Figure 5) may reflect variations in Fe(III)/Fe(II) or total Fe composition among individual grains and/or varying degrees of electron beam damage. For example, Ahn and Peacor (1986) pointed out that variations in layer spacings in oxidized smectite have been attributed to heterogeneity in local composition and therefore in interlayer charge. Furthermore, Drits and Manceau (2000) mentioned that a small amount of ferric iron does not effectively disturb the crystal-lattice stabilization energy and the layer charge is compensated predominantly by the sorption of Na.

Slade *et al.* (1991) identified ~1.8 nm and ~1.5 nm XRD 001 peaks of various smectites in NaCl solutions as corresponding to three and two H<sub>2</sub>O planes in the interlayer, respectively. Further, Keeling *et al.* (2000) identified ~1.5 nm, ~1.3 nm and ~1.0 nm XRD 001 peaks of Ca-saturated, dried (105°C, 24 h) N<sub>Au</sub>-1 and N<sub>Au</sub>-2 nontronite as corresponding to two, one or no H<sub>2</sub>O plane(s) in the interlayer, respectively. Therefore, our measurements are consistent with the assertion that the EC-TEM holder maintained our N<sub>Au</sub>-1 nontronite in a hydrated state, *i.e.* that hydrated interlayers were present. Although it is difficult to quantify precisely the degree of hydration of the specimens in the EC, the hydration conditions during imaging of both the non-reduced and reduced nontronite should be largely equivalent. Therefore, differences observed in basal layer spacings between non-reduced and reduced nontronite can be attributed to microbial effects, most likely those of Fe(III) reduction.

Changes in the nontronite SAED patterns (Figure 3) from diffuse rings to rather discrete Bragg reflections following Fe(III) reduction suggest an increase in the

order of face-to-face stacking arrangements. This is further supported by XRD results (Figure 6). Reduction of Fe(III) may increase the net negative charge on clay surfaces. Extracellular biopolymers (polysaccharides, lipids, and organic acids), secreted by bacteria, are also net negatively charged, yet they bind readily to substrates including clays, with surface tension probably dominating over electrostatic repulsion. In culture suspensions, biopolymers may facilitate reordering of individual clay sheets since they attract cations while also acting as glue holding mutually repulsing clay sheets in close proximity. Clay sheets attracted to the same set of cations in the biopolymer could reorient to reduce their total free energy forming a new layer stacking.

In conclusion, the main advantage of EC-TEM is that clays can be investigated in their hydrated state, eliminating artifacts resulting from dehydration and sample infiltration. We showed that established embedding techniques used to study clay reduction do not accurately preserve basal spacings of expandable clays. At least for the L.R. White resin technique, solvent exchange and resin infiltration modify layer spacings, and therefore cannot be used to study, for example, the correlation between layer spacing and local Fe(III)/Fe(II) composition. The Nanoplast resin technique avoids solvent exchange and reduces artifacts of resin infiltration, though it does not prevent layer contraction caused by dehydration during TEM observation. In fact, conventional TEM has been unable to image conclusively the contraction of clay layers induced by Fe(III) reduction.

This paper demonstrates proof of principle, laying the groundwork for more detailed direct studies of hydrated clays. In this regard, techniques have been developed to determine the oxidation state of 3d and 4d transition metals using EELS-measured L<sub>2,3</sub> (Leapman *et al.*, 1982; Colliex *et al.*, 1991; van Aken *et al.*, 1998), and M<sub>2,3</sub> (van Aken *et al.*, 1999) adsorption edges. We are presently using EELS to study Fe(III)/Fe(II) ratios in individual nontronite grains and that will provide further valuable information on microbial reduction of clays. For the study of clay layer structure, EC-TEM is indeed the essential tool for which clay mineralogists have searched for several years.

#### ACKNOWLEDGMENTS

This work was funded by NRL/ONR base funding program element No. 0601153N, CORE/NRL Postdoctoral Fellowship, and the US Navy. We thank Dr J. Kostka of Florida State University for providing us with *S. oneidensis*, Jan Watkins of NRL for helping with the experiments and Al Falster of the Geology department at the University of New Orleans for assisting with the XRD measurements. This is NRL contribution No. 7430-02-2.

#### REFERENCES

Ahn, J.H. and Peacor, D.R. (1986) Transmission and analytical electron microscopy of the smectite-to-illite transformation.

- Clays and Clay Minerals*, **34**, 165–179.
- Biscaye, P.E. (1965) Mineralogy and sedimentation of recent deep sea clay in the Atlantic Ocean and adjacent seas and oceans. *Geological Society of America Bulletin*, **76**, 803–832.
- Chen, S.Z., Low, P.F. and Roth, C.B. (1987) Relation between potassium fixation and oxidation state of octahedral iron. *Soil Science Society of America Journal*, **51**, 82–86.
- Colliex, C., Manoubi, T. and Ortiz, C. (1991) Electron-energy-loss-spectroscopy near-edge fine structures in the iron-oxygen system. *Physical Review*, **B44**, 11402–11411.
- Daulton, T.L., Little, B.J., Lowe, K. and Jones-Meehan, J. (2001) In-situ environmental cell-transmission electron microscopy study of microbial reduction of chromium(VI) using electron energy loss spectroscopy. *Journal of Microscopy and Microanalysis*, **7**, 470–485.
- Drits, V.A. and Manceau, A. (2000) A model for the mechanism of Fe(III) to Fe(II) reduction in dioctahedral smectites. *Clays and Clay Minerals*, **48**, 185–195.
- Egashira, K. and Ohtsubo, M. (1983) Swelling and mineralogy of smectites in paddy soils derived from marine alluvium, Japan. *Geoderma*, **29**, 119–127.
- Foster, M.D. (1953) Geochemical studies of clay minerals: II. Relation between ionic substitution and swelling in montmorillonites. *American Mineralogist*, **38**, 994–1006.
- Fukami, A., Fukushima, K. and Kohyama, N. (1991) Observation technique for wet clay minerals using film-sealed environmental cell equipment attached to a high-resolution electron microscope. Pp. 321–331 in: *Microstructure of Fine-grained Sediments from Mud to Shale* (R.H. Bennett, W.R. Bryant, M.H. Hulbert, editors). Springer-Verlag, New York.
- Gates, W.P., Wilkinson, H.T. and Stucki, J.W. (1993) Swelling properties of microbially reduced ferruginous smectite. *Clays and Clay Minerals*, **41**, 360–364.
- Keeling, J.L., Raven, M.D. and Gates, W.P. (2000) Geology and characterization of two hydrothermal nontronites from weathered metamorphic rocks at the Uley graphite mine, South Australia. *Clays and Clay Minerals*, **48**, 537–548.
- Keller, M.D., Bellows, W.K. and Guillard, R.L. (1988) Microwave treatment for sterilization of phytoplankton culture media. *Journal of Experimental Marine Biology and Ecology*, **117**, 279–283.
- Khaled, E.M. and Stucki, J.W. (1991) Effect of iron oxidation state on cation fixation in smectites. *Soil Science Society of America Journal*, **55**, 550–554.
- Kim, J.W., Peacor, D.R., Tessier, D. and Elsass, F. (1995) A technique for maintaining texture and permanent expansion of smectite interlayers for TEM observations. *Clays and Clay Minerals*, **43**, 51–57.
- Kohyama, N., Shimoda, S. and Sudo, T. (1973) Iron-rich saponite (ferrous and ferric forms). *Clays and Clay Minerals*, **21**, 229–237.
- Kostka, J.E., Haefele, E., Viehweger, R. and Stucki, J.W. (1999) Respiration and dissolution of iron (III)-containing clay minerals by bacteria. *Environmental Science and Technology*, **33**, 3127–3133.
- Kostka, J.E., Stucki, J.W., Nealson, K.H. and Wu, J. (1996) Reduction of structural Fe(III) in smectite by a pure culture of *Shewanella Putrefaciens* strain MR-1. *Clays and Clay Minerals*, **44**, 522–529.
- Leapman, R.D., Gunes, L.A. and Fejes, P.L. (1982) Study of the  $L_{23}$  edges in the 3d transition metals and their oxides by electron-energy-loss spectroscopy with comparisons to theory. *Physical Review*, **B 26**, 614–635.
- Lear, P.R. and Stucki, J.W. (1989) Effects of iron oxidation state on the specific surface area of nontronite. *Clays and Clay Minerals*, **37**, 547–552.
- Lee, J.H. and Peacor, D.R. (1986) Expansion of smectite by laurylamine hydrochloride: Ambiguities in transmission electron microscope observations. *Clays and Clay Minerals*, **34**, 69–73.
- Leppard, G.G., Heissenberger, A. and Herndl, G.J. (1996) Ultrastructure of marine snow. I. Transmission electron microscopy methodology. *Marine Ecology Progress Series*, **135**, 289–298.
- Myers, C.R. and Nealson, K.H. (1988) Bacterial manganese reduction and growth with manganese oxide as the sole electron acceptor. *Science*, **240**, 1319–1321.
- Ravina, I. and Low, P.F. (1972) Relation between swelling, water properties and *b*-dimension with swelling of montmorillonite. *Clays and Clay Minerals*, **20**, 109–123.
- Ravina, I. and Low, P.F. (1977) Change of *b*-dimension with swelling of montmorillonite. *Clays and Clay Minerals*, **25**, 196–200.
- Shen, S., Stucki, J.W. and Boast, C.W. (1992) Effects of structural iron reduction on the hydraulic conductivity of Na-smectite. *Clays and Clay Minerals*, **40**, 381–386.
- Slade, P.G., Quirk, J.P. and Norrish, K. (1991) Crystalline swelling of smectite samples in concentrated NaCl solutions in relation to layer charge. *Clays and Clay Minerals*, **39**, 234–238.
- Stucki, J.W. and Tessier, D. (1991) Effects of iron oxidation state on the texture and structural order of Na-nontronite gels. *Clays and Clay Minerals*, **39**, 137–143.
- Stucki, J.W., Low, P.F., Roth, C.B. and Golden, D.C. (1984) Effects of oxidation state of octahedral iron on clay swelling. *Clays and Clay Minerals*, **32**, 357–362.
- Stucki, J.W., Komadel, P. and Wilkinson, H.T. (1987) Microbial reduction of structural iron(III) in smectites. *Soil Science Society of America Journal*, **51**, 1663–1665.
- Tessier, D. (1984) Etude experimentale de l'organisation des materiaux argileux: Hydratation, gonflement et structuration au cours de a desiccation et de la rehumection. Ph.D. thesis, University of Paris, France, 361 pp.
- van Aken, P.A., Liebscher, B. and Styrsa, V.J., (1998) Quantitative determination of iron oxidation states in minerals using Fe  $L_{2,3}$ -edge electron energy-loss near-edge structure spectroscopy. *Physics and Chemistry of Minerals*, **25**, 323–327.
- van Aken, P.A., Styrsa, V.J., Liebscher, B., Woodland, A.B., Redhammer, G.J. (1999) Microanalysis of Fe<sup>3+</sup>/ΣFe in oxide and silicate minerals by investigation of electron energy-loss near-edge structures (ELNES) at the Fe  $M_{2,3}$  edge. *Physics and Chemistry of Minerals*, **26**, 584–590.
- Wu, J., Roth, C.B. and Low, P.F. (1988) Biological reduction of structural iron in Na-nontronite. *Soil Science Society of America Journal*, **52**, 295–296.
- Wu, J., Low, P.F. and Roth, C.B. (1989) Effects of octahedral-iron reduction and swelling pressure on interlayer distances in Na-nontronite. *Clays and Clay Minerals*, **37**, 211–218.

(Received 6 September 2002; revised 20 January 2003; Ms. 712; A.E. Peter J. Heaney)